CrystEngComm

Accepted Manuscript

ROYAL SOCIETY OF CHEMISTRY

www.rsc.org/crystengcomm

CrystEngComm

ARTICLE

Incorporation of single-walled aluminosilicate nanotubes for the control of crystal size and porosity in zeolitic imidazolate framework-L †

Received 18th October 2015,
Accepted 00th January 20xx

DOI: 10.1039/x0xx00000x

www.rsc.org/

An-Chih Yang,[a] Ting-Yu Wang,[b] Chi-An Dai [a] and Dun-Yen Kang*[a]

Zeolitic imidazolate framework-L (ZIF-L) is an emerging ZIF material possessing a unique two-dimensional layered crystal structure and leaf-like crystal morphology. This paper reports a novel approach to the incorporation of single-walled aluminosilicate nanotubes (AlSiNTs) into the interlayer of ZIF-L, which is formed by hydrogen bonding between adjacent imidazoles in the synthesis of AlSiNT@ZIF-L nanocomposites. The resulting nanocomposites were subjected to a number of solid-state characterization techniques (SEM, TEM, powder XRD, EDS, TGA, nitrogen physisorption, and FT-IR) to elucidate the conformation of their microstructure. It was found that AlSiNT@ZIF-L composite possesses an average crystal size considerably smaller than that of pure ZIF-L (1.1 µm for AlSiNT@ZIF-L and 7.8 µm for pure ZIF-L). Interestingly, ZIF-L and AlSiNTs are both microporous; however, this characteristic was achieved through the incorporation of AlSiNTs into ZIF-L crystals. A control experiment related to the synthesis of AlSiNT@ZIF-8 composites was performed to gain insight into the assembly pathway to the formation of AlSiNT@ZIF-L crystals. Failure in the formation of AlSiNT@ZIF-8 supports the supposition that the assembly pathway involves the incorporation of AlSiNTs into the interlayer of ZIF-L, thereby facilitating the nucleation of ZIF-L crystals.

1. Introduction

Zeolitic imidazolate frameworks (ZIFs) are an emerging subclass of metal-organic framework (MOF) with ordered micropores (pore size < 2 nm).[1-3] The highly tunable pore topology and interior surface properties make ZIFs promising candidates for molecular separation.[4-8] Zeolitic imidazolate framework-L (ZIF-L) is a novel ZIF material (firstly synthesized in 2013)[9] possessing a unique two-dimensional layered crystal morphology (Figs. 1a and 1b). ZIF-L is a pseudopolymorph of ZIF-8 [10]; both of which are composed of zinc and 2-methyl imidazole. However, unlike ZIF-L, ZIF-8 has a regular, nearly spherical crystal morphology. The layered crystal structure of ZIF-L is formed by the stacking of 2D nanosheets along the c-direction via the hydrogen bonds formed between adjacent imidazoles.[9, 11] Furthermore, ZIF-L exhibits a higher CO_2 adsorption capacity than does ZIF-8.[9, 11, 12]

One well-known approach to engineering the intrinsic properties of MOFs involves hybridization with other classes of nanomaterials to create nanocomposites. Nanotubes are a nanomaterial that has been used for this kind of hybridization with MOF materials.[13-17] Several studies have reported the hybridization of nanocomposites using MOFs and carbon nanotubes (CNTs). Prasanth et al.[18] incorporated single-walled CNTs into MIL-101 to synthesize a hybrid composite with the ability to tune the pore size and volume. H_2 storage at room temperature was enhanced by blending CNT with MOF-5.[19] Dumee et al.[20] synthesized ZIF-8-CNT composite membranes to enhance N_2 selectivity over CO_2 and Xe. Despite successes in the

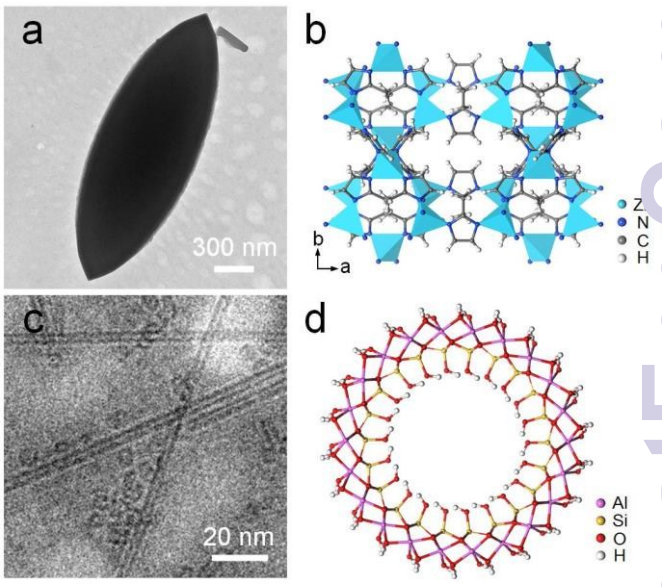

Fig. 1. (a) TEM image and (b) crystal structure of ZIF-L; (c) Cryo-TEM

[a] Department of Chemical Engineering, National Taiwan University, Taipei, Taiwan. *E-mail: dunyen@ntu.edu.tw
[b] Electron Microscope Unit of Instrument Center, National Taiwan University, Taipei, Taiwan.

†Electronic Supplementary Information (ESI) available: SEM and TEM images, simulated XRD patterns, FT-IR spectra, XRD patterns of ZIF-L, ZIF-8 and their corresponding composites. See DOI: 10.1039/x0xx00000x

hybridization of MOF and CNT in achieving desirable material properties, the high synthesis costs of CNTs shed doubt on the large-scale applicability of these nanocomposites. Metal oxide nanotubes, which can be synthesized hydrothermally or solvothermally, may provide an alternate nanotube material.[21, 22] Among the various types of metal oxide nanotube, single-walled aluminosilicate nanotubes have drawn particular attraction in recent years (Figs. 1c and 1b).[23-29] These nanotubes are synthetic analogues of the nanotubular mineral imogolite. The external surface of AlSiNTs are covered by hydroxyl groups (Fig. 1d), which make them amenable to aqueous-phase processing and compatible with hydrophilic materials as well as materials with a surface/interface capable of forming hydrogen bonds with hydroxyls.[25, 30, 31] The pore size of AlSiNTs is approximately 1 nm, which make them an excellent candidate for catalysis,[32] molecular storage,[24, 33, 34] and separation.[30] Nonetheless, no previous study has reported nanocomposite materials composed of AlSiNTs and MOFs.

In this paper, we present the first synthesis of nanocomposite hybridization using ZIF-L and AlSiNTs. In this process, the crystal size and the porosity of ZIF-L can be controlled through the incorporation of AlSiNTs within ZIF-L crystals. Comprehensive material characterization of the proposed AlSiNT@ZIL-L nanocomposites was performed using a number of solid-state techniques, including scanning electron microscopy (SEM), transmission electron microscopy (TEM), dispersive energy spectroscopy (EDS), X-ray diffraction (XRD), thermogravimetric analysis (TGA), nitrogen physisorption, and Fourier transform infrared spectroscopy (FT-IR). In our attempts to synthesize AlSiNT@ZIL-8 composites, important insights were gained into the assembly pathways of AlSiNT@ZIL-L nanocomposites.

2. Experimental

2.1 Synthesis of AlSiNTs

Aluminum-tri-sec-butoxide was mixed with tetraethyl orthosilicate (TEOS) in a glove box filled with nitrogen. The mixture was immediately added to 0.038 M perchloric acid solution at a molar ratio of Si:Al:$HClO_4$ = 1:2:1 at room temperature and maintained under stirring for 24 h. Following this aging stage, the solution was diluted by a factor of 3.8 using DI water and refluxed at 95 ^oC for 4 days. When the temperature reached 95 ^oC, the solution turned from turbid to transparent within 1 h. Following four days of stirring, the suspension was cooled to ambient temperature and concentrated using a rotary evaporator to various concentrations (0.1, 0.5, 1.0 and 2.0 wt%). The resulting solutions were purified using a 12 kDa dialysis membrane against DI water for 3 days. The purified solutions were then ready for the preparation of AlSiNT@ZIF nanocomposites.

2.2 Synthesis of AlSiNT@ZIF Nanocomposites

AlSiNT@ZIF-L composites were prepared using a modification of the procedure reported in our previous work.[35] In a typical synthesis process, 0.9669 g (11.6 mmole) of 2-methylimidazole (MeIm) was added to 25 g of AlSiNT solution. The mixture was stirred for 2 h at room temperature until MeIm was fully dissolved. A separate solution was then prepared by adding 0.4381 g (1.46 mmole) of zinc nitrate ($Zn(NO_3)_2 \cdot 6H_2O$) to 5 g of DI water. This solution was slowly dropped into the MeIm-AlSiNT mixture and maintained under stirring at room temperature for 4 h. The molar ratio of the Zn:MeIm:H_2O in the final mixture was 1:8:1143. The resulting solution was subjected to centrifugation at 11,000 rpm for 30 min. The supernatant was discarded and the precipitate was washed using methanol. This purification procedure was repeated three times. The resulting solid-state product comprising AlSiNT@ZIF-L nanocomposites was stored in a convective oven at 105 ^oC prior to use. AlSiNT@ZIF-L nanocomposites synthesized using the 0.1, 0.5, 1.0 and 2.0 wt% solutions were denoted as AlSiNT@ZIF-L(0.1%), AlSiNT@ZIF-L(0.5%), AlSiNT@ZIF-L(1.0%) and AlSiNT@ZIF-L(2.0%), respectively. Pure ZIF-L as a control sample was synthesized using the procedure mentioned above, except for the substitution of AlSiNT aqueous solution with DI water (i.e. 0% of AlSiNT solution).

We then sought to synthesize AlSiNT@ZIF-8 nanocomposites using the same procedures employed in the synthesis of AlSiNT@ZIF-L, except that the molar ratio of Zn:MeIm was changed to 1:70.

To examine the effect of water quantity on the morphology of ZIF-L, we varied the total quantity of water as follows: 60 g, 30 g, 15 g, and 5 g (molar ratio of Zn:H_2O=1:2286, Zn:H_2O=1:1143, Zn:H_2O=1:572 and Zn:H_2O=1:190, respectively).

2.3 Characterization

Powder X-ray diffraction (XRD) patterns were obtained using a Rigaku diffractometer (40 kV, 40 mA) with Cu Kα radiation at a scanning rate of 2^o min^{-1} from 2^o to 40^o 2θ with a step size of 0.02^o. The morphology of all solid-state samples was characterized using a Hitachi S-4800 Field Emission scanning electron microscope (SEM) with Energy Dispersive Spectrometer (EDS) operated at an accelerated voltage of 15 kV. The average crystal size of the samples was estimated by post-processing SEM images using the free software ImageJ.[36, 37] Regular and cryogenic transmission electron microscopy (cryo-TEM) images were obtained using an FEI T-12 equipped with a field gun at 120 kV. Thermogravimetric analysis (TGA) was performed using a PerkinElmer's Pyris 1 with approximately 5 mg of the samples under nitrogen diluted air. During testing, the temperature was elevated from room temperature to 800 ^oC at a ramp rate of 10 ^oC/min. Nitrogen physisorption isotherms were obtained using a Micromeritics ASAP 2010 analyzer at 77 K. Prior to physisorption measurement, the samples were placed in an analysis tube and degassed under 20 torr at 200 ^oC overnight. FT-IR spectra were acquired using a JASCO FT/IR-6700 spectrometer with a Ge coated KBr beam splitter. Each FT-IR spectrum was obtained from 100 scans at a resolution of 4 cm^{-1}.

3. Results and discussion

3.1 Crystal Morphology AlSiNT@ZIF-L Nanocomposites

SEM and TEM images as well as the energy dispersive spectra of ZIF-L and AlSiNT@ZIF-L(1.0%) nanocomposites are summarized in Fig. 2. The AlSiNT@ZIF-L nanocomposites present the same leaf-like crystal morphology as pure ZIF-L, which suggest that the presence of AlSiNTs does not inhibit the crystallization of ZIF-L and does not affect the crystal shape of ZIF-L. However, we observed a remarkable difference in crystal size (taken as the length along the long axis of the leaf-like crystal) between ZIF-L and AlSiNT@ZIF-L(1.0%): the average crystal size of ZIF-L is 5.0 μm (Figs. 2b and 2d), whereas the crystal size of AlSiNT@ZIF-L(1.0%) is 1.4 μm (Figs. 2a and 2c). The reduction in crystal size induced by the incorporation of AlSiNTs into ZIF-L implies that the AlSiNTs participate in the either the nucleation or crystallization of ZIF-L. One plausible assembly pathway in the formation of AlSiNT@ZIF-L(1.0%) is detailed in the following sections. As shown in the SEM (Fig. 2d) and TEM (Fig. 2f) images, the surfaces of pure ZIF-L appear fairly smooth. In contrast, heterogeneous structures were observed in the SEM (Fig. 2c) and TEM (Fig. 2e) images of AlSiNT@ZIF-L(1.0%). The formation of these heterogeneous structures is likely due to the incorporation of AlSiNTs into ZIF-L crystals. Single nanotubes and bundles of nanotubes are more easily observed in the high-magnification TEM and SEM images of AlSiNT@ZIF-L(1.0%) (Supplementary Information, Fig. S1) In addition, EDS analysis (Figs. 2g and 2h) revealed pronounced Si and Al peaks in the spectrum of AlSiNT@ZIF-L(1.0%), which suggests the presence of AlSiNTs. In contrast, Si and Al signals are absent from the spectra of pure ZIF-L. In summary, EM and EDS characterization strongly indicates the successful embedding of AlSiNTs in AlSiNT@ZIF-L nanocomposites.

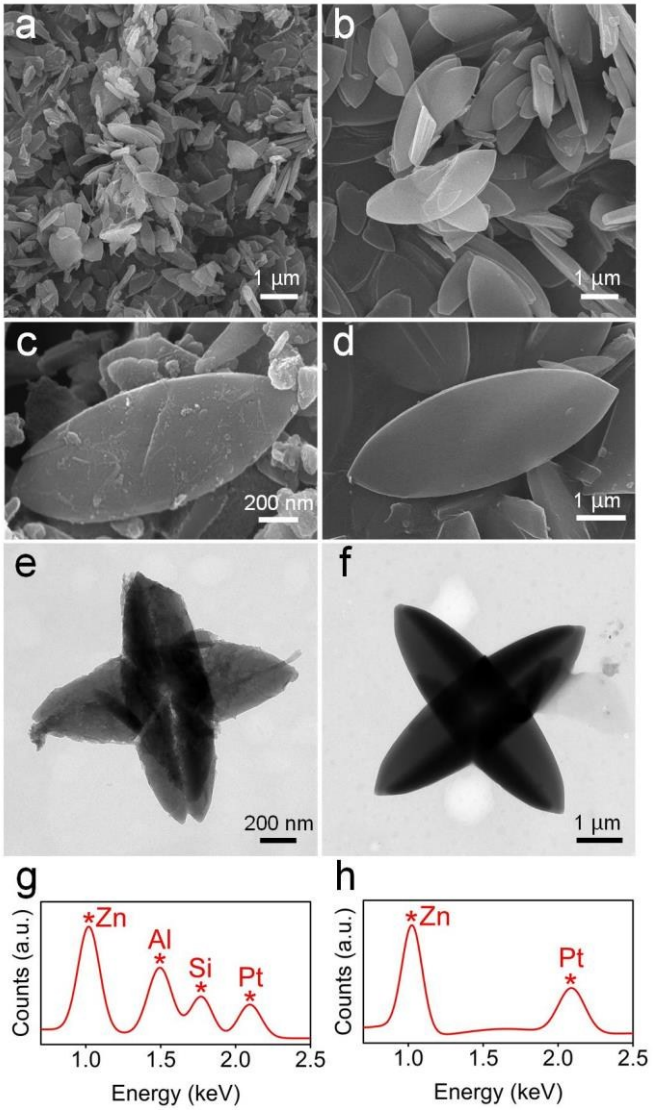

Fig. 2. Low-magnification SEM images of (a) AlSiNT@ZIF-L(1.0%) and (b) ZIF-L; High-magnification SEM images of (c) AlSiNT@ZIF-L(1.0%) and (d) ZIF-L; TEM images of (e) AlSiNT@ZIF-L(1.0%) and (f) ZIF-L. EDS spectra of (g) AlSiNT@ZIF-L(1.0%) and (h) ZIF-L.

3.2 Crystallinity, Composition, and Porosity of AlSiNT@ZIF-L

Figure 3 summarizes the powder XRD patterns of pure ZIF-L, pure AlSiNTs, and AlSiNT@ZIF-L(1.0%). The pattern from as-synthesized AlSiNTs indicates the scattering form factor of the small nanotube bundles, which is in good agreement with previously reported findings.[25] The XRD patterns of ZIF-L obtained in this study are also consistent with those presented in previous studies.[9, 11, 20] The characteristics of AlSiNTs as well as ZIF-L were observed in the XRD patterns of AlSiNT@ZIF-L. This provides further evidence (in addition to EM and EDS) of the successful incorporation of AlSiNTs into the ZIF-L crystals resulting in the formation of AlSiNT@ZIF-L composites. The comparison between the experimental and simulated XRD patterns (Supplementary Information, Fig. S2) suggests that the incorporated AlSiNTs are likely to form small bundles in ZIF-L.

Fig. 4 presents a summary of the thermogravimetric analysis (TGA) of as-synthesized ZIF-L, as-synthesized AlSiNTs, and AlSiNT@ZIF-L(1.0%). The TGA curves of ZIF-L [9] and AlSiNTs [25, 30] are consistent with the findings of previous studies. We were operating under the assumption that residual AlSiNT at

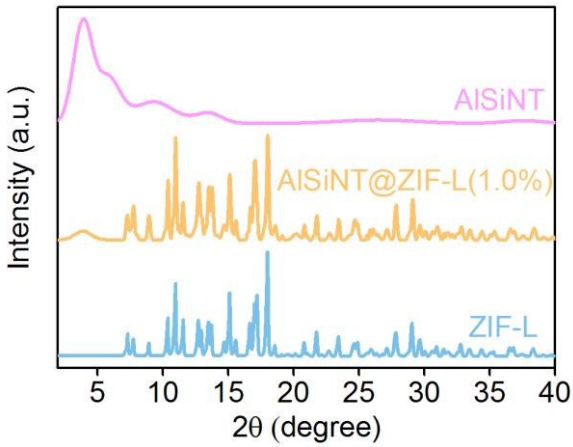

Fig. 3. Powder XRD patterns of AlSiNT@ZIF-L(1.0%), AlSiNT and ZIF-L.

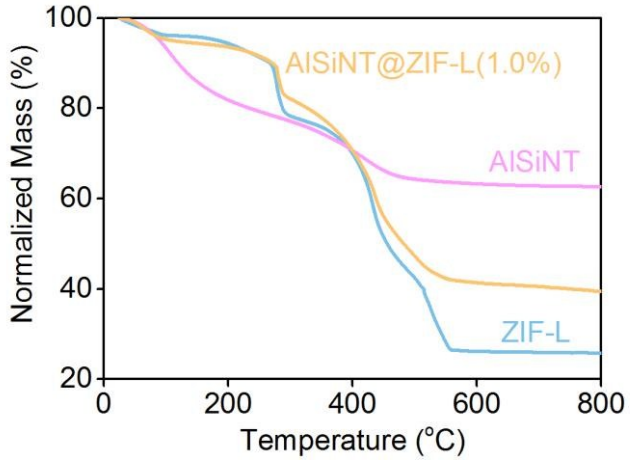

Fig. 4. TGA results of AlSiNT@ZIF-L(1.0%), AlSiNT and ZIF-L.

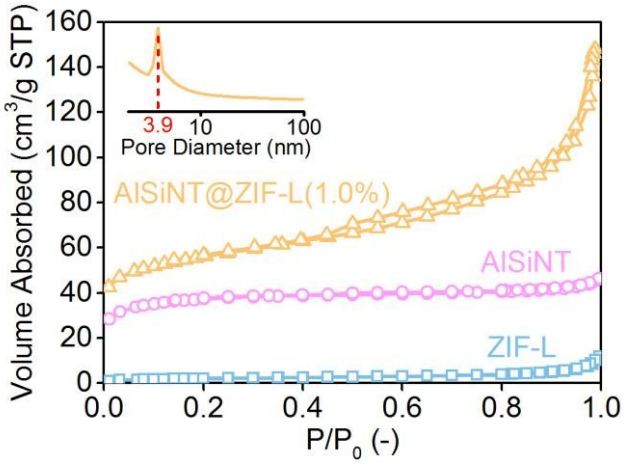

Fig. 5. Nitrogen physisorption isotherms of AlSiNT@ZIF-L(1.0%), AlSiNT and ZIF-L. The inset shows the deduced pore size distribution of AlSiNT@ZIF-L(1.0%).

the conclusion of combustion has an empirical formula of $Al_2O_3SiO_2$,[30] and that the ZIF-L sample has an empirical formula of ZnO.[9] Based on these assumptions, the molar ratio of Zn to Al deduced from the TGA mass loss curve of AlSiNT@ZIF-L was Zn:Al:Si=1:2.2:1.1. This derived value is close to the Zn-to-Al molar ratio associated with the synthesis of AlSiNT@ZIF-L (1:2). The FT-IR spectra of ZIF-L, AlSiNTs, and AlSiNT@ZIF-L are summarized in the Supplementary Information (Fig. S3). Consistent with XRD and TGA characterization, the FT-IR spectrum of AlSiNT@ZIF-L(1.0%) presents the characteristics of ZIF-L as well as AlSiNTs.

Figure 5 presents nitrogen physisorption isotherms of ZIF-L, AlSiNTs, and AlSiNT@ZIF-L(1.0%). As-made ZIF-L [9, 11, 20, 35] showed relatively low microporosity and AlSiNTs [24, 25, 34] showed typical microporosity. Both findings are in good agreement with those of previous reports. The AlSiNT@ZIF-L presented a micropore volume slightly higher than pure AlSiNTs. ZIF-L is nearly nonporous; therefore, the microporosity of AlSiNT@ZIF-L(1.0%) nanocomposites may very well be attributed solely to the inclusion of AlSiNTs, which could create nanoconfinement in the miropore region. Interestingly, hysteresis between the adsorption and desorption isotherms was observed in the AlSiNT@ZIF-L(1.0%) sample, which is an indication of mesoporosity. The deduced pore size distribution suggests a pore size of 3.9 nm. The derived surface area and pore volumes are summarized in the Supplementary Information (Table S1). The literature includes very few instances of mesoporosity in composites comprising two microporous materials. The mesoporosity of AlSiNT@ZIF-L(1.0%) is likely due to the heterogeneous interface between AlSiNTs and ZIF-L crystals.

3.3 Assembly pathway and microstructure of AlSiNT@ZIF-L

To gain further insight into the assembly pathway of AlSiNTs@ZIF-L, the same nanocomposite was synthesized

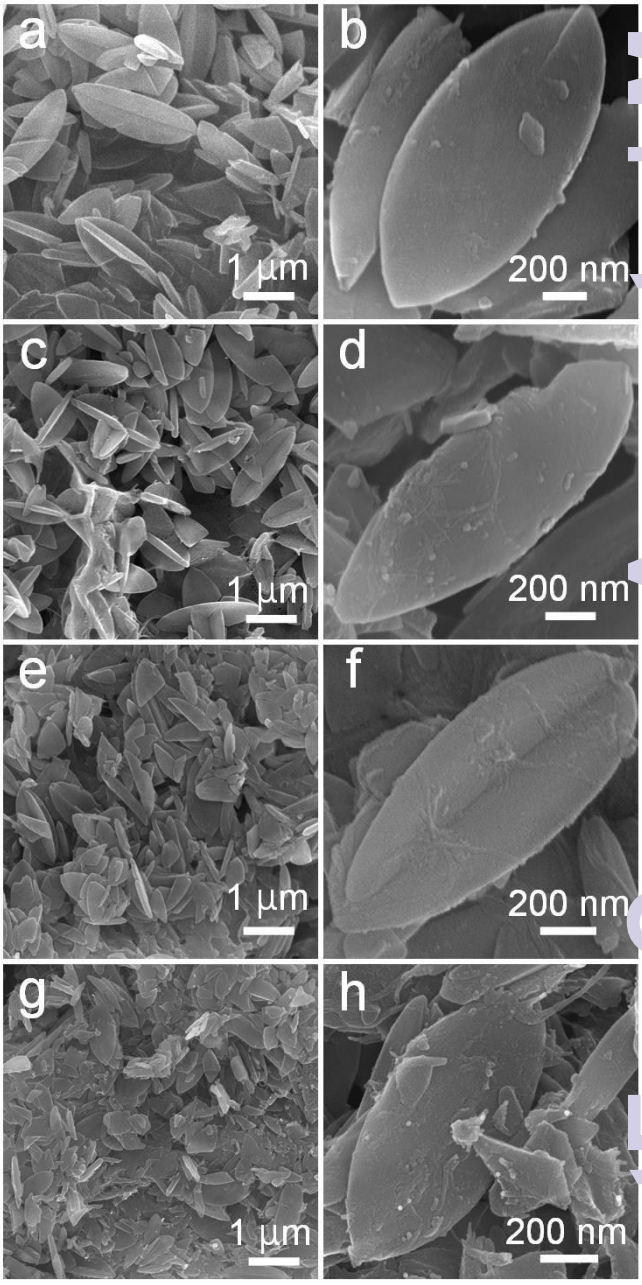

Fig. 6. SEM images of (a) and (b) AlSiNT@ZIF-L(0.1%), (c) and (d) AlSiNT@ZIF-L(0.5%), (e) and (f) AlSiNT@ZIF-L(1.0%), and (g) and (h) AlSiNT@ZIF-L(2.0%).

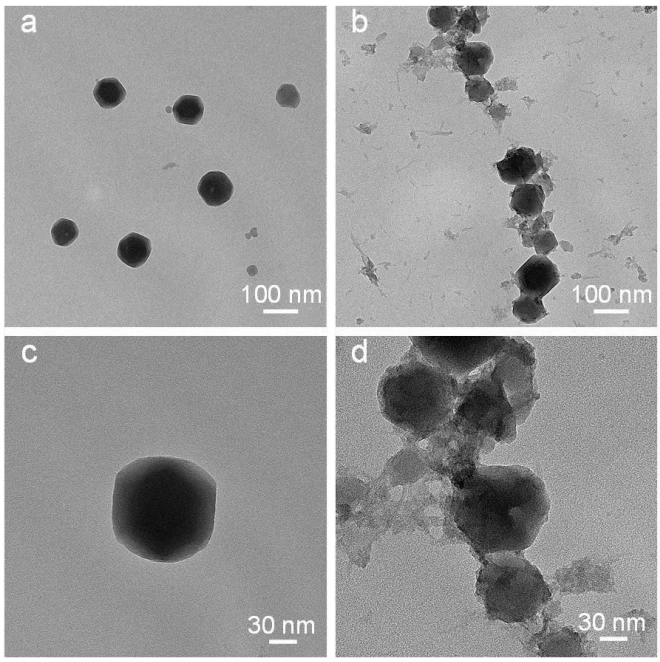

Fig. 7. Low-magnification TEM images of (a) pure ZIF-8 and (b) the product of our attempt at synthesizing AlSiNT@ZIF-8(1.0%) using a similar method for synthesizing the AlSiNT@ZIF-L. High-magnification TEM images of (c) pure ZIF-8 and (d) the product of our attempt at synthesizing AlSiNT@ZIF-8(1.0%).

using various concentrations of AlSiNT solutions. We then investigated the crystal morphology and interlayer distance of the resulting composites. Figure 6 presents SEM images of AlSiNTs@ZIF-L synthesized using various AlSiNT solutions. It was observed that the size of nanocomposite crystals monotonically decreased with an increase in the concentration of the AlSiNT solutions. The average size of crystals were as follows: AlSiNT@ZIF-L(0.1%): 2.3 μm, AlSiNT@ZIF-L(0.5%): 1.8 μm, AlSiNT@ZIF-L(1.0%):1.4 μm, and AlSiNT@ZIF-L(2.0%) 1.1 μm. The average crystal sizes were determined by post-processing raw SEM images using ImageJ software.[36, 37] XRD patterns (Fig. S4 in Supplementary Information) of these nanocomposites revealed a monotonic increases in the relative intensity of nanotube patterns (between 3-5° 2θ with an increase in the concentration of the AlSiNT solutions used in the synthesis of the composites. This is an indication of the incorporation of AlSiNTs into the composites.

The decrease in crystal size in the nanocomposites with an increase in AlSiNT concentration may be due entirely to the decrease in water content. In other words, if two AlSiNT solutions with the same mass were used in separate synthesis batches, the solution with the higher AlSiNT concentration would have a lower water content, as reported previously.[38] To avoid this possibility, we synthesized pure ZIF-L in solutions using a variety of Zn:H_2O ratios (1:2286, 1:1143, 1:572, and 1:190). SEM images and XRD patterns of these samples are summarized in the Supplementary Information (Figs. S5 and S6 respectively). The average crystal sizes of ZIF-L(Zn:H_2O=1:2286), ZIF-L(Zn:H_2O=1:1143), and ZIF-L(Zn:H_2O=1:572) were 7.8, 5.0, and 3.9 μm respectively. The crystal morphology of ZIF-L(Zn:H_2O=1:190) was poorly defined; therefore we opted not to estimate the average crystal size. The smallest crystal size achieved by decreasing the water content in the synthesis solution was 3.9 μm, in which the Zn-to-H_2O ratio was 1:572. However, in the synthesis solution with 0.1 wt% of AlSiNTs in water with a Zn-to-H_2O ratio of 1:1143, we obtained an average crystal size as small as 2.3 μm. This is an indication that the inclusion of AlSiNTs in the synthesis solution is a more effective means of reducing the crystal size of ZIF-L than is decreasing the water content. This observation also helps to explain why the decrease in the crystal size of AlSiNT@ZIF-L following an increase of the concentration of the AlSiNT solution cannot be attributed solely to a decrease in water content. We hypothesize that the AlSiNTs serve as nuclei for the crystallization of ZIF-L, such that a higher concentration of nuclei in the solution would typically result in crystals of smaller size.

One explanation for the AlSiNTs acting as nuclei in the crystallization of ZIF-L may be the unique layered structure of ZIF-L crystals. Specifically, ZIF-L crystals are 2D nanosheets stacked one on the other in the c-direction via hydrogen bonds, rather than covalent bonds, between adjacent imidazoles. AlSiNTs have abundant hydroxyl groups on the external surface, which could be involved in the formation of hydrogen bonds with imidazole, resulting in their incorporation into the interlayer of ZIF-L crystals. To test this hypothesis, we sought to employ the composite synthesis method used for AlSiNT@ZIF-L in the synthesis of AlSiNT@ZIF-8(1.0%) nanocomposite, wherein ZIF-8 is a pseudopolymorph of ZIF-L but with a crystal framework made entirely of covalent bonds. TEM images of the resulting products are presented in Fig. 7 and the XRD patterns are presented in the Supplementary Information (Fig. S7). In the TEM images, no differences were observed between the resulting AlSiNT@ZIF-8(1.0%) and pure ZIF-8 with regard to crystal size. More importantly, the AlSiNTs appear to have formed in the AlSiNT@ZIF-8(1.0%) nanocomposite a phase distinct from that of ZIF-8, which suggests a failure to synthesis this composite. The fact that only covalent bonds are involved in the framework of ZIF-8 crystals makes it nearly impossible to incorporate AlSiNTs. This supports our speculation that the incorporation of AlSiNTs within the interlayer of ZIF-L crystals

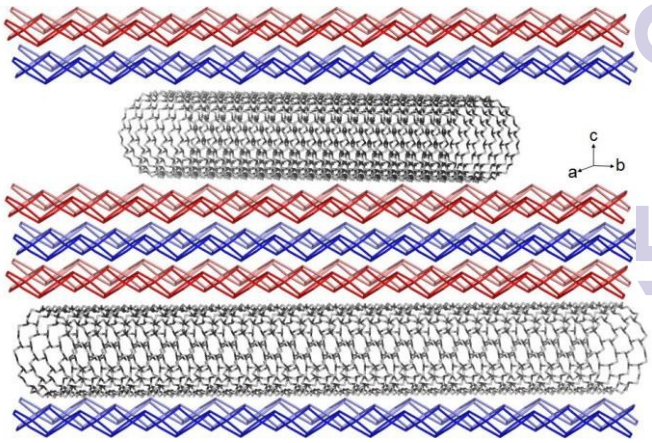

Fig. 8. Proposed microstructure of AlSiNT@ZIF-L nanocomposite.

involves the formation of hydrogen bonds with the imidazole in ZIF-L. Specifically, the difference between the pseudopolymorph ZIF-L and ZIF-8 in with regard to crystal structure is the stacking of nanosheets along the c-axis through the formation of hydrogen bonds in ZIF-L. The proposed microstructure of AlSiNT@ZIF-L is presented in Fig. 8.

4. Conclusions

In conclusion, this study succeeded in the synthesis of AlSiNT@ZIF-L nanocomposites through the incorporation of AlSiNTs into ZIF-L crystals. Synthesis was performed using aqueous solutions of AlSiNT. The resulting nanocomposites preserved the 2D leaf-like crystal morphology of ZIF-L. Our success in the synthesis of AlSiNT@ZIF-L nanocomposites was confirmed using a number solid-state characterization techniques, including SEM, TEM, EDS, powder XRD, TGA, nitrogen physisorption, and FT-IR. We determined that the incorporation of AlSiNTs into ZIF-L leads to a reduction in the crystal size of ZIF-L (from 7.8 to 1.1 μm). ZIF-L and AlSiNTs are both microporous materials; however, it was interesting to note the occurrence of mesoporosity in the AlSiNT@ZIF-L. To elucidate the assembly pathway involved in the formation of AlSiNT@ZIF-L, we attempted the synthesis of AlSiNT@ZIF-8 composite using a similar method for synthesizing the AlSiNT@ZIF-L composites; however, this attempt failed. This failure to synthesize AlSiNT@ZIF-8 suggests that the AlSiNTs may be incorporated within the interlayer spacing of ZIF-L along the c-axis. This spacing does not exist in ZIF-8 crystals. It appears that the incorporation of AlSiNTs may facilitate the nucleation of ZIF-L, resulting in a decrease in the crystal size of ZIF-L. This is the first report pertaining to AlSiNT@ZIF nanocomposite. We expect that these findings may open up new possibilities for the use of AlSiNT materials in engineering the intrinsic properties of metal organic frameworks and/or zeolitic imidazolate frameworks.

Acknowledgements

This work was supported by the Ministry of Science and Technology (MOST) of Taiwan (MOST 104-2628-E-002-009-MY3 and MOST 104-2218-E-002-006) and National Taiwan University (NTU-CDP-104R7814). We would like to thank Chin-Yan Lin, Wu-Chihs and Ya-Yun Yang in the Electron Microscope Unit of Instrument Center at National Taiwan University for helping us to obtain SEM images. We would also like to thank Professor Huanting Wang at Monash University for generously providing CIF files of ZIF-L crystals.

Notes and references

1. R. Banerjee, A. Phan, B. Wang, C. Knobler, H. Furukawa, M. O'Keeffe and O. M. Yaghi, Science, 2008, 319, 939-943.
2. B. Wang, A. P. Cote, H. Furukawa, M. O/'Keeffe and O. M. Yaghi, Nature, 2008, 453, 207-211.
3. H. Hayashi, A. P. Cote, H. Furukawa, M. O/'Keeffe and O. M. Yaghi, Nat. Mater., 2007, 6, 501-506.
4. Y. Ban, Y. Li, Y. Peng, H. Jin, W. Jiao, X. Liu and W. Yang, Chem. Eur. J., 2014, 20, 11402-11409.
5. V. I. Isaeva, M. I. Barkova, L. Kustov, D. A. Syrtsova, E. Efimova and V. Teplyakov, J. Mater. Chem. A, 2015, 3, 7469-7476.
6. A. Kasik, X. Dong and Y. S. Lin, Microporous Mesoporous Mater., 2015, 204, 99-105.
7. R. Banerjee, H. Furukawa, D. Britt, C. Knobler, M. O'Keeffe and O. M. Yaghi, J. Am. Chem. Soc., 2009, 131, 3875-3877.
8. A. Huang, H. Bux, F. Steinbach and J. Caro, Angew. Chem., 2010, 122, 5078-5081.
9. R. Chen, J. Yao, Q. Gu, S. Smeets, C. Baerlocher, H. Gu, D. Zhu, W. Morris, O. M. Yaghi and H. Wang, Chem. Commun., 2013, 49, 9500-9502.
10. Z.-X. Low, J. Yao, Q. Liu, M. He, Z. Wang, A. K. Suresh, J. Bellare and H. Wang, Cryst. Growth Des., 2014, 14, 6589-6598.
11. Z. Zhong, J. Yao, R. Chen, Z. Low, M. He, J. Z. Liu and H. Wang, J. Mater. Chem. A, 2015, 3, 15715-15722.
12. B. Motevalli, H. Wang and J. Z. Liu, J. Phys. Chem. C, 2015, 119, 16762-16768.
13. R. S. Rahul, A. Heejoon, K. Jung Ho and Y. Yusuke, Nanotechnology, 2015, 26, 204004.
14. M. Anbia and S. Sheykhi, J. Ind. Eng. Chem., 2013, 19, 1583-1586.
15. W. Bao, Z. Zhang, C. Zhou, Y. Lai and J. Li, J. Power Sources, 2014, 248, 570-576.
16. H. Lee, Y. N. Choi, S. B. Choi, J. H. Seo, J. Kim, I. H. Cho, S. Gang and C. H. Jeon, J. Phys. Chem. C, 2014, 118, 5691-5699.
17. E. Zhou, Y. Zhang, Y. Li and X. He, Electroanalysis, 2014, 26, 2526-2533.
18. K. P. Prasanth, P. Rallapalli, M. C. Raj, H. C. Bajaj and R. V. Jasra, Int. J. Hydrogen Energy, 2011, 36, 7594-7601.
19. S. J. Yang, J. Y. Choi, H. K. Chae, J. H. Cho, K. S. Nahm and C. R. Park, Chem. Mater., 2009, 21, 1893-1897.
20. L. Dumee, L. He, M. Hill, B. Zhu, M. Duke, J. Schutz, F. She, H. Wang, S. Gray, P. Hodgson and L. Kong, J. Mater. Chem. A, 2013, 1, 9208-9214.
21. R. Tenne and C. N. R. Rao, Phil. Trans. R. Soc. A, 2004, 362, 2099-2125.
22. C. Rao and A. Govindaraj, Adv. Mater., 2009, 21, 4208-4233.
23. I. Bottero, B. Bonelli, S. E. Ashbrook, P. A. Wright, W. Zhou, M. Tagliabue, M. Armandi and E. Garrone, Phys. Chem. Chem. Phys., 2011, 13, 744-750.
24. D.-Y. Kang, N. A. Brunelli, G. I. Yucelen, A. Venkatasubramanian, J. Zang, J. Leisen, P. J. Hesketh, C. W. Jones and S. Nair, Nat. Commun., 2014, 5.
25. D.-Y. Kang, J. Zang, E. R. Wright, A. L. McCanna, C. W. Jones and S. Nair, ACS Nano, 2010, 4, 4897-4907.
26. K.-H. Liou, N.-T. Tsou and D.-Y. Kang, Nanoscale, 2015, 7, 16222-16229.
27. A. Thill, P. Maillet, B. Guiose, O. Spalla, L. Belloni, P. Chaurand, M. Auffan, L. Olivi and J. Rose, J. Am. Chem. Soc., 2012, 134, 3780-3786.

28. G. I. Yucelen, D.-Y. Kang, R. C. Guerrero-Ferreira, E. R. Wright, H. W. Beckham and S. Nair, Nano Lett., 2012, 12, 827-832.
29. J. Zang, S. Chempath, S. Konduri, S. Nair and D. S. Sholl, J. Phys. Chem. Lett., 2010, 1, 1235-1240.
30. D.-Y. Kang, H. M. Tong, J. Zang, R. P. Choudhury, D. S. Sholl, H. W. Beckham, C. W. Jones and S. Nair, ACS Appl. Mat. Interfaces, 2012, 4, 965-976.
31. D.-Y. Kang, M. E. Lydon, G. I. Yucelen, C. W. Jones and S. Nair, Chem. Nano. Mat., 2015, 1, 102-108.
32. B. Bonelli, I. Bottero, N. Ballarini, S. Passeri, F. Cavani and E. Garrone, J. Catal., 2009, 264, 15-30.
33. B. Bonelli, M. Armandi and E. Garrone, Phy. Chem. Ch. Ph., 2013, 15, 13381-13390.
34. D.-Y. Kang, J. Zang, C. W. Jones and S. Nair, J. Phys. Chem. C, 2011, 115, 7676-7685.
35. W.-C. Lee, H.-T. Chien, Y. Lo, H.-C. Chiu, T.-p. Wang and D.-Y. Kang, ACS Appl. Mater. Inter., 2015, 7, 18353-18361.
36. M. D. Abràmoff, P. J. Magalhães and S. J. Ram, Biophotonics international, 2004, 11, 36-42.
37. C. A. Schneider, W. S. Rasband and K. W. Eliceiri, Nature methods, 2012, 9, 671-675.
38. X. Gu, K. Zhou, Y. Feng and J. Yao, Chem. Lett., 2015, 44, 1080-1082.

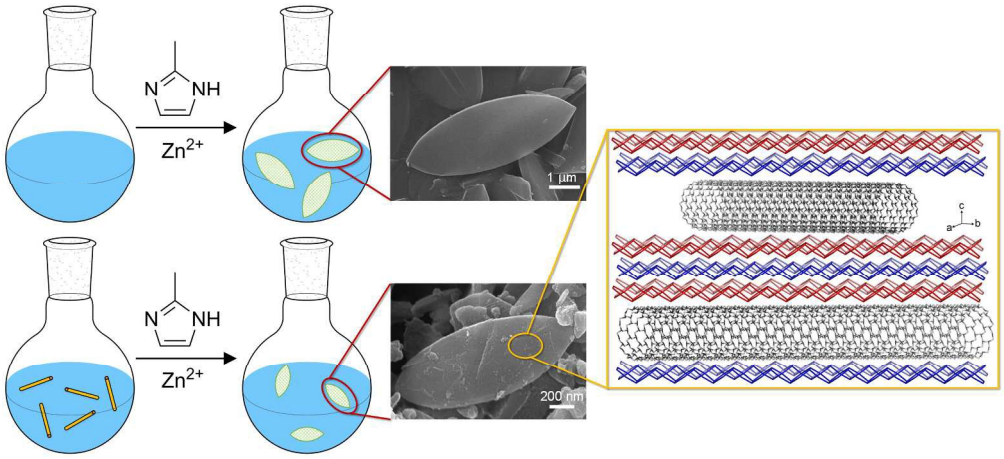

646x293mm (100 x 100 DPI)